

Amphetamine actions at the serotonin transporter rely on the availability of phosphatidylinositol-4,5-bisphosphate

Florian Buchmayer^{a,1}, Klaus Schicker^{a,1}, Thomas Steinkellner^a, Petra Geier^a, Gerald Stübiger^a, Peter J. Hamilton^b, Andreas Jurik^c, Thomas Stockner^a, Jae-Won Yang^a, Therese Montgomery^{a,d}, Marion Holy^a, Tina Hofmaier^a, Oliver Kudlacek^a, Heinrich J. G. Matthies^b, Gerhard F. Ecker^c, Valery Bochkov^a, Aurelio Galli^b, Stefan Boehm^{a,2}, and Harald H. Sitte^{a,2,3}

^aCenter of Physiology and Pharmacology, Medical University Vienna, A-1090 Vienna, Austria; ^bDepartment of Molecular Physiology and Biophysics, Center for Molecular Neuroscience, Kennedy Center, Vanderbilt University, Nashville, TN 37013; ^cDepartment of Medicinal Chemistry, University of Vienna, A-1090 Vienna, Austria; and ^dSchool of Biomolecular and Biomedical Science, University College Dublin, Dublin 4, Ireland

Edited* by Susan G. Amara, National Institute of Mental Health, Bethesda, MD, and approved May 31, 2013 (received for review December 19, 2012)

Nerve functions require phosphatidylinositol-4,5-bisphosphate (PIP₂) that binds to ion channels, thereby controlling their gating. Channel properties are also attributed to serotonin transporters (SERTs); however, SERT regulation by PIP₂ has not been reported. SERTs control neurotransmission by removing serotonin from the extracellular space. An increase in extracellular serotonin results from transporter-mediated efflux triggered by amphetamine-like psychostimulants. Herein, we altered the abundance of PIP₂ by activating phospholipase-C (PLC), using a scavenging peptide, and inhibiting PIP₂-synthesis. We tested the effects of the verified scarcity of PIP₂ on amphetamine-triggered SERT functions in human cells. We observed an interaction between SERT and PIP₂ in pull-down assays. On decreased PIP₂ availability, amphetamine-evoked currents were markedly reduced compared with controls, as was amphetamine-induced efflux. Signaling downstream of PLC was excluded as a cause for these effects. A reduction of substrate efflux due to PLC activation was also found with recombinant noradrenaline transporters and in rat hippocampal slices. Transmitter uptake was not affected by PIP₂ reduction. Moreover, SERT was revealed to have a positively charged binding site for PIP₂. Mutation of the latter resulted in a loss of amphetamine-induced SERT-mediated efflux and currents, as well as a lack of PIP₂-dependent effects. Substrate uptake and surface expression were comparable between mutant and WT SERTs. These findings demonstrate that PIP₂ binding to monoamine transporters is a prerequisite for amphetamine actions without being a requirement for neurotransmitter uptake. These results open the way to target amphetamine-induced SERT-dependent actions independently of normal SERT function and thus to treat psychostimulant addiction.

phosphoinositide | reuptake | release | mass spectrometry | amperometry

Phosphoinositides are concentrated within the inner leaflets of plasma membranes where they serve as membrane anchors for cytoplasmic proteins and as signaling molecules (1). Phosphatidylinositol-4,5-bisphosphate (PIP₂) is produced by 1-phosphatidylinositol 4-kinase (PI-4 kinase) and PIP-5 kinase through the sequential phosphorylation of phosphatidylinositol. PIP₂ is the precursor of two important second messengers: inositol triphosphate (IP₃) and diacylglycerol [DAG (2)]. These two PIP₂ products result from cleavage by phospholipase C (PLC) that is activated via receptors coupled to PLC. IP₃ stimulates Ca²⁺ release from the endoplasmic reticulum, whereas DAG directly activates most of the known protein kinase C isoforms. However, PIP₂ is not only a precursor for second messengers but is also by itself important for signaling as it serves as an anchor for protein kinase C (3), directly binds to various membrane proteins (1), and is enriched in membrane rafts (4). Thereby, PIP₂ controls essential functions of neurons, such as exocytosis (5), endocytosis (6), and transmembrane ion fluxes (7, 8).

Ion fluxes have also been observed in neurotransmitter:sodium symporters (NSSs). Members of this protein family, such as the transporters for dopamine (DAT), norepinephrine (NET), serotonin (5HT; SERT), and GABA (GAT), mediate uptake of released neurotransmitters from the synaptic cleft. In addition, they are targets for addictive drugs such as amphetamines (9). Ion fluxes through these proteins are required for amphetamine-evoked substrate efflux but not for transmitter reuptake (10).

In contrast to neuronal ion channels and ion transporters, NSSs have not been reported to be regulated by PIP₂, although other plasma membrane constituents such as cholesterol are required for the proper function of SERT (11–13) and DAT (14). Herein, we reveal SERT as a unique binding partner of membrane PIP₂, characterize the binding site involved, and show that PIP₂ is necessary for amphetamine actions but not for substrate reuptake. By targeting this interaction, one could thus prevent the contribution of SERT to addiction without affecting its physiological function.

Results and Discussion

Plasma Membrane PIP₂ Is Required for SERT-Mediated Current. An interaction between PIP₂ and SERT was established using PIP₂-coated beads and proteins solubilized from human embryonic kidney 293 (HEK293) cells stably expressing the human SERT (HEK-SERT cells; Fig. 1A) (15). The direct interaction of PIP₂ with ion channels and exchange proteins is required to permit ion fluxes in those proteins (8, 16). To test for analogous phenomena in SERT, currents through this transporter were triggered by the application of a substrate such as *para*-chloroamphetamine (*p*CA) (17). To disrupt PIP₂ interactions, a palmitoylated peptide was used (Pal-HRQKHFEKRR; 10 μM), which is known to inhibit the effects of PIP₂ on ion channels by binding to its polar head groups (18). This peptide reduced the *p*CA-induced SERT-mediated currents (Fig. 1B; 82.9 ± 5.1% inhibition; *n* = 4). A scrambled

Author contributions: F.B., K.S., T. Steinkellner, G.S., P.J.H., A.J., T. Stockner, J.-W.Y., T.M., O.K., H.J.G.M., G.F.E., V.B., A.G., S.B., and H.H.S. designed research; F.B., K.S., T. Steinkellner, P.G., G.S., P.J.H., A.J., T. Stockner, J.-W.Y., T.M., M.H., T.H., O.K., and H.J.G.M. performed research; F.B., K.S., T. Steinkellner, P.G., G.S., P.J.H., A.J., T. Stockner, J.-W.Y., T.M., M.H., T.H., O.K., H.J.G.M., G.F.E., V.B., A.G., S.B., and H.H.S. analyzed data; and F.B., K.S., T. Steinkellner, P.G., G.S., P.J.H., A.J., T. Stockner, J.-W.Y., T.M., M.H., O.K., H.J.G.M., G.F.E., V.B., A.G., S.B., and H.H.S. wrote the paper.

The authors declare no conflict of interest.

*This Direct Submission article had a prearranged editor.

Freely available online through the PNAS open access option.

¹F.B. and K.S. contributed equally to this work.

²S.B. and H.H.S. contributed equally to the work.

³To whom correspondence should be addressed. E-mail: harald.sitte@meduniwien.ac.at.

This article contains supporting information online at www.pnas.org/lookup/suppl/doi:10.1073/pnas.1220552110/-DCSupplemental.

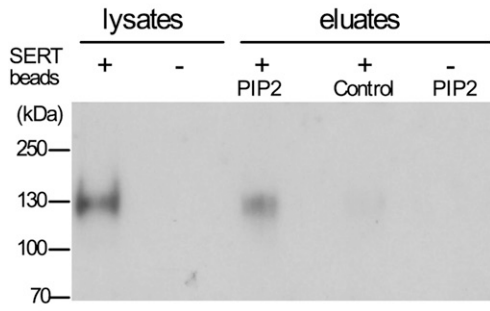


Fig. 1. PIP₂ binding to SERT and regulation of SERT-mediated currents. (A) Lysates of either HEK293 cells expressing YFP-SERT (+) or nontransfected HEK293 (-) cells were incubated with either PIP₂-coated beads or control beads. Samples of these lysates or proteins eluted from these beads were separated by SDS/PAGE and immunoblotted with an anti-GFP antibody. (B–G) Current traces from single HEK293-SERT cells; application of pCA (3 μM) is indicated by the bar: traces were obtained in the presence (gray) and absence (black; Ctl) of 10 μM pal-HRQKHFEKRR (pal-peptide in B), 10 μM scrambled peptide (C), 10 μM m-3M3FBS (D), 10 μM o-3M3FBS (E), 10 μM m-3M3FBS plus 3 μM U73122 (F), or 10 nM bradykinin (G). The peptides, m-3M3FBS, o-3M3FBS, m-3M3FBS plus U73122, or 10 nM bradykinin had been present for 20 min before the currents were recorded. Cells in G were coexpressing B₂ bradykinin receptors. (Calibration bars, 2 pA and 2 s.)

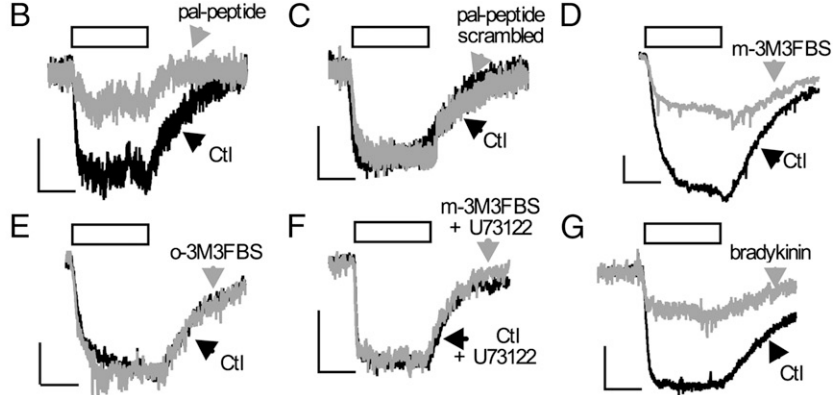
peptide (PAL-HAQKHFEAAA; 10 μM) unable to bind PIP₂ did not exert any effect on SERT-mediated currents (Fig. 1C).

We used the specific PLC activator *m*-3M3FBS {2,4,6-trimethyl-*N*-(3-(trifluoromethyl)phenyl)benzenesulfonamide} (19) to deplete membrane-associated PIP₂. In cells treated with *m*-3M3FBS (10 μM) for 10 min, PIP₂ contents were reduced to 49 ± 4% in comparison with cells treated with *o*-3M3FBS, an inactive ortho-analog, as quantified by MALDI-TOF (Fig. S14). *m*-3M3FBS (10 μM) led to a significant decrease in pCA-induced SERT-mediated currents (Fig. 1D; 58.3 ± 8.9% inhibition; *n* = 7), whereas *o*-3M3FBS had no such effect (Fig. 1E; 6.8 ± 5.3% inhibition; *n* = 7). SERT-mediated current is not only induced by amphetamines such as pCA but also by the physiological substrate 5HT itself (20). Application of *m*-3M3FBS, but not *o*-3M3FBS, significantly reduced 5HT-induced currents (74.6 ± 8.1% inhibition, *n* = 4). Cells were treated with the PLC inhibitor U73122 to confirm that the effect of *m*-3M3FBS was caused by an activation of PLC; thereafter, *m*-3M3FBS failed to affect pCA-induced currents (0.1 ± 0.02% inhibition, *n* = 4; Fig. 1F).

To activate PLC by physiological means, B₂ bradykinin receptors (B₂R) were expressed in HEK-SERT cells, activation of which is known to tightly control the PIP₂ content of the plasma membrane by PLC-mediated hydrolysis (21). pCA-induced current was significantly reduced by 59.6 ± 7.7% (*n* = 5) on addition of bradykinin (Fig. 1G). This effect was mediated by B₂R activation because coapplication of the B₂R-specific antagonist Hoe 140 (100 nM) attenuated the B₂R-mediated effect on the SERT current (9.9 ± 3.8% inhibition, *n* = 5; sample trace in Fig. S1B). Thus, SERT interacts with PIP₂ and amphetamine induced currents through the transporter can be altered by reducing PIP₂ or by interfering with PIP₂-protein interactions.

PIP₂ Depletion Inhibits SERT-Mediated Efflux but Not Influx. Currents through NSS family members are carried by sodium ions (22), and this sodium influx is believed to trigger transporter-mediated substrate efflux (23, 24). Therefore, the consequences of disrupting SERT-PIP₂ interactions by the interfering palpeptide were also tested with respect to reverse transport using single cell microamperometry as previously described for DAT (24). Amperometric signals from HEK-SERT cells patch-loaded with 5HT were significantly reduced in the presence of 10 μM palpeptide (Fig. 2A, *n* = 6; *P* < 0.05, two-tailed Student *t* test).

This result raises the question of whether 5HT uptake might also be affected by modulating PIP₂ levels: PIP₂ levels were



reduced by *m*-3M3FBS, but not *o*-3M3FBS, as reported above (Fig. 1D). As uptake cannot be measured in single cells, these experiments were carried out in populations of HEK-SERT cells. Neither agent induced significant alterations compared with vehicle (Table S1). In addition to [³H]substrate uptake, we also examined pCA uptake as quantified by HPLC (25). Thereby, we ruled out that the pCA that is used as the trigger for transporter-mediated efflux may be differently handled by the transporter: again, neither *m*-3M3FBS nor *o*-3M3FBS had any significant effect (867.4 ± 112.2 and 843.6 ± 124.8 pmol/100 μL, respectively; *n* = 4). The disparity between PIP₂-sensitive SERT-mediated current (Fig. 1) and -insensitive uptake supports previous observations of uncoupled ion fluxes through SERT (20), which may additionally require an interaction with syntaxin 1A (22).

HEK-SERT cells were preloaded with the nondegradable substrate, tritiated methyl-4-phenylpyridinium (MPP⁺), and continuously superfused until a baseline was established. SERT-dependent [³H]MPP⁺ efflux was induced by pCA (3 μM) (26) and measured by liquid scintillation counting. *m*-3M3FBS reduced this efflux in a concentration-dependent manner (Fig. 2B). Again, *o*-3M3FBS had no effect (Fig. 2B). The inhibitory action of *m*-3M3FBS was attenuated by the PLC inhibitor U73122 (5 μM; Fig. 2C).

PI-4-kinase is involved in the synthesis of PIP₂; its inhibition causes effects similar to those of PLC activation, but it is independent of PLC activity and products (27). Superfusion of [³H]MPP⁺-loaded HEK-SERT cells with phenyl-arsenoxide (PAO; 30 μM), a PI-4-kinase inhibitor, for 10 min before the addition of pCA resulted in a reduction of pCA-induced efflux (Fig. 2C; *n* = 12–16, *P* < 0.001 compared with control; one-way ANOVA, followed by Tukey's post hoc test).

In cells coexpressing B₂R, the addition of bradykinin (10 nM) significantly reduced pCA-triggered efflux (Fig. 2D; *P* < 0.05 compared with control; one-way ANOVA, followed by Tukey's post hoc test), which was prevented by the B₂R antagonist Hoe 140 (100 nM; Fig. 2D). Thus, depletion of membrane PIP₂ through PLC-dependent or -independent mechanisms, or interference with PIP₂ protein interactions, reduced transporter-mediated sodium currents and substrate efflux. PIP₂ sensitivity of [³H]MPP⁺ efflux was also found with the norepinephrine transporter: *m*-3M3FBS reduced d-amphetamine-induced efflux from HEK293-NET cells (Fig. 2E; *n* = 3). Furthermore, the physiological significance of our findings can be demonstrated by the sensitivity of pCA-induced [³H]MPP⁺-efflux from rat hippocampal slices

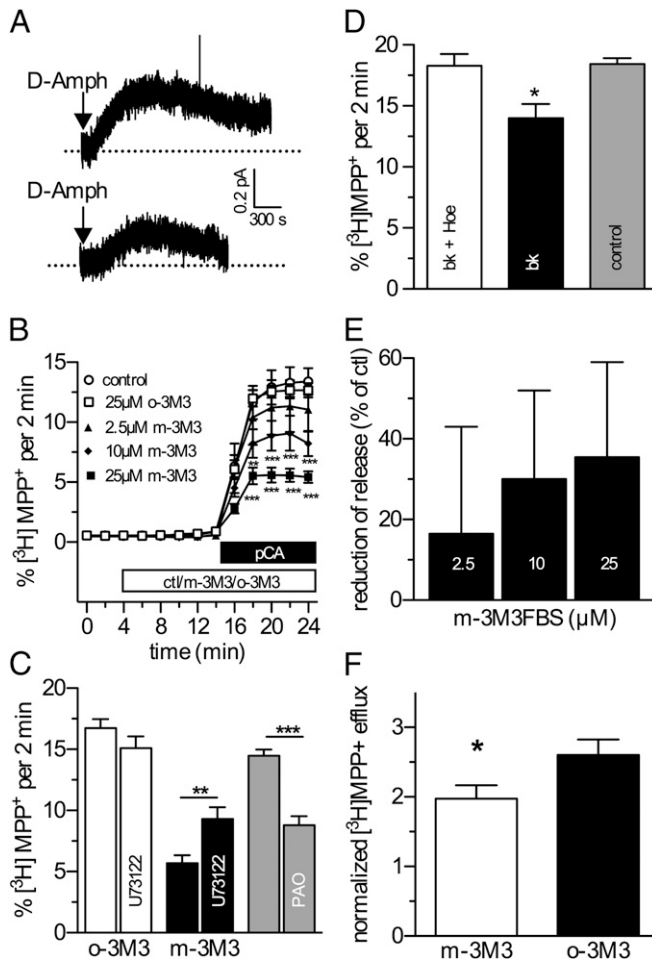


Fig. 2. PIP₂ regulation of SERT-mediated efflux. (A) Representative oxidative currents from HEK-SERT cells. D-Amph (10 μ M) was added as indicated by the arrows. Traces were obtained from cells loaded with either 10 μ M scrambled peptide (upper trace) or pal-HRQKHFEKFR (lower trace). (B) Time course of pCA-induced, SERT-mediated efflux of [3 H]MPP $^+$ from HEK-SERT cells. The cells were loaded with 0.1 μ Ci [3 H]MPP $^+$ and superfused, and 2-min fractions were collected. The indicated concentrations of *m*-3M3FBS or 25 μ M *o*-3M3FBS were added to the superfusion buffer at minute 4. At minute 14, pCA (3 μ M) was added to induce efflux. Efflux of radioactivity per 2-min fraction is expressed as percentage of radioactivity present in the cells at the beginning of that fraction ($n = 6$; two-way ANOVA followed by Bonferroni's post hoc test: ** $P < 0.01$ or *** $P < 0.001$). (C) Experiments were carried out as shown in B; 25 μ M *m*-3M3FBS or *o*-3M3FBS, in the absence or presence of 3 μ M U73122, was added at minute 4. Similarly, 30 μ M PAO was compared against control. Bar graphs represent efflux in percent of total radioactivity between minutes 22 and 24 ($n = 5-37$; two-tailed Mann-Whitney test: ** $P < 0.01$ or *** $P < 0.001$). (D) Experiments were carried out as shown in B; pCA-induced, SERT-mediated efflux of [3 H]MPP $^+$ from HEK-SERT cells coexpressing B₂ bradykinin receptors. Bradykinin (10 nM), either alone or together with 100 nM Hoe 140, was added to the superfusion buffer at minute 4. At minute 14, pCA (3 μ M) was added to induce efflux ($n = 3$; one-way ANOVA followed by Bonferroni's post hoc test and is denoted by * $P < 0.05$).

Panel E: Concentration dependence of *m*-3M3FBS treatment on the reduction of efflux in HEK293-DAT or HEK293-NET cells ($n = 3$; D-amphetamine, 3 μ M). Cells were treated essentially as described in B.

Panel F: Rat hippocampal slices were preloaded with 0.1 μ M [3 H]MPP $^+$, and SERT-mediated efflux was induced by 3 μ M pCA in the presence of *m*-3M3FBS or *o*-3M3FBS. Nomifensine (100 nM) was present throughout the experiment to block potential contributions from NET and DAT. Efflux is presented as in C-E. Statistically significant differences were assessed by Student *t* test ($P < 0.05$; $n = 6$, performed in triplicate).

toward PIP₂ hydrolysis by *m*-3M3FBS (Fig. 2F). Thus, activation of PLC affected efflux through both recombinant and natively expressed monoamine transporters.

Second-Messenger Systems Are Activated but Do Not Contribute to PIP₂ Effects on SERT: PKC and Ca²⁺. Cleavage of PIP₂ by PLC yields DAG, which activates PKC, leading to translocation from the cytosol to the membrane. The PKC- β II isoform is the most relevant for amphetamine-induced phosphorylation of transporters (28), and PKC is involved in the initiation of transporter-mediated efflux (25). In HEK-SERT cells, *m*-3M3FBS, but not *o*-3M3FBS, translocated recombinant fluorescent β II PKC to the membrane (Fig. S2A), indicative of PKC activation. Moreover, the PKC inhibitor GF109203X (1 μ M) significantly diminished SERT-mediated efflux (Fig. S2B), but failed to alter the PIP₂-dependent inhibition of efflux by *m*-3M3FBS (Fig. S2B). Thus, and apparently counterintuitive, the observed change in PKC activity on PLC activation by *m*-3M3FBS cannot be accounted for as the reason for the pronounced reduction in pCA-induced efflux.

PLC activation also increases the concentration of IP₃, which in turn triggers the release of Ca²⁺ from intracellular stores after binding to IP₃ receptors; Ca²⁺ may play a role in transporter-mediated efflux as previously reported for the DAT (29). However, incubation of HEK-SERT cells with the membrane permeant Ca²⁺ chelator BAPTA-AM (50 μ M) did not affect pCA-induced [3 H]MPP $^+$ efflux, whether *m*-3M3FBS was present or not (Fig. S2C). Likewise, the inhibition of pCA-induced current by *m*-3M3FBS was not altered by BAPTA-AM (control: 27.71 \pm 11.42% vs. in the presence of BAPTA-AM: 31.6 \pm 6.4%, $n = 5$; $P > 0.05$, Mann-Whitney *U* test). Thus, changes in intracellular Ca²⁺ did not mediate the effects of PLC activation on amphetamine-induced currents and efflux.

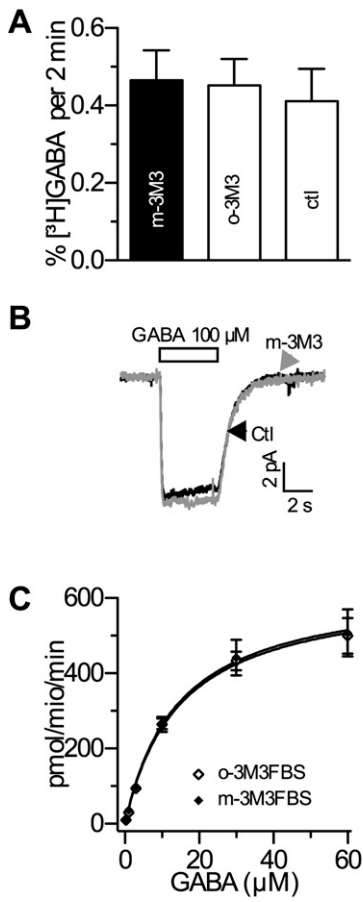
Apart from shifting monoamine transporters from a reluctant to a willing state in terms of efflux, PKC also induces redistribution from the cell surface to intracellular compartments (30). However, within an exposure time of 20 min, neither *m*-3M3FBS nor *o*-3M3FBS led to the internalization of SERT in confocal microscopy and cell surface biotinylation experiments (Fig. S2D and E). Nevertheless, activation of PKC by β -PMA significantly reduced cell surface expression of SERT as shown by biotinylation and a reduction in the V_{max} of 5HT uptake (Fig. S2F; $P < 0.05$, $n = 4$; paired two-tailed Student *t* test). Thus, the PIP₂ hydrolysis products, IP₃ and DAG, were not involved in the modulation of transporter-mediated currents and efflux by PLC activation, indicating that the loss of PIP₂ was the decisive mechanism.

PIP₂ Does Not Regulate GAT1 Activity, Another Member of the NSS Family.

We investigated substrate efflux through the GABA transporter GAT1, a more distantly related member of the NSS family (31), to learn whether the above results might be universally valid for all NSSs. However, release of [3 H]GABA from HEK cells stably expressing rat GAT1 (HEK-GAT1 cells) remained unaffected even at the highest *m*-3M3FBS concentrations tested (Fig. 3A). Likewise, GABA-evoked currents in HEK-GAT1 cells were not affected by 10 μ M *m*-3M3FBS (Fig. 3B). Nevertheless, the PIP₂ levels of HEK-GAT1 cells were decreased after application of *m*-3M3FBS (Fig. S3) to an extent comparable to those in HEK-SERT cells (Fig. 1D). Thus, GABA transporters are insensitive toward changes in PIP₂ levels as suggested earlier (16), but it must be mentioned that GAT1 is insensitive to amphetamines, and specific “releasers” have not been identified for GAT1 (26).

The sequence identity between SERT and GAT1 is low (~20%) (31). Therefore, the apparent differences in PIP₂ sensitivity might be based on structural heterogeneities. Ion channels bind PIP₂ via positively charged intracellular domains (33). Hence, we compared the electrostatic potentials of GAT1 and SERT (Fig. 3D and E).

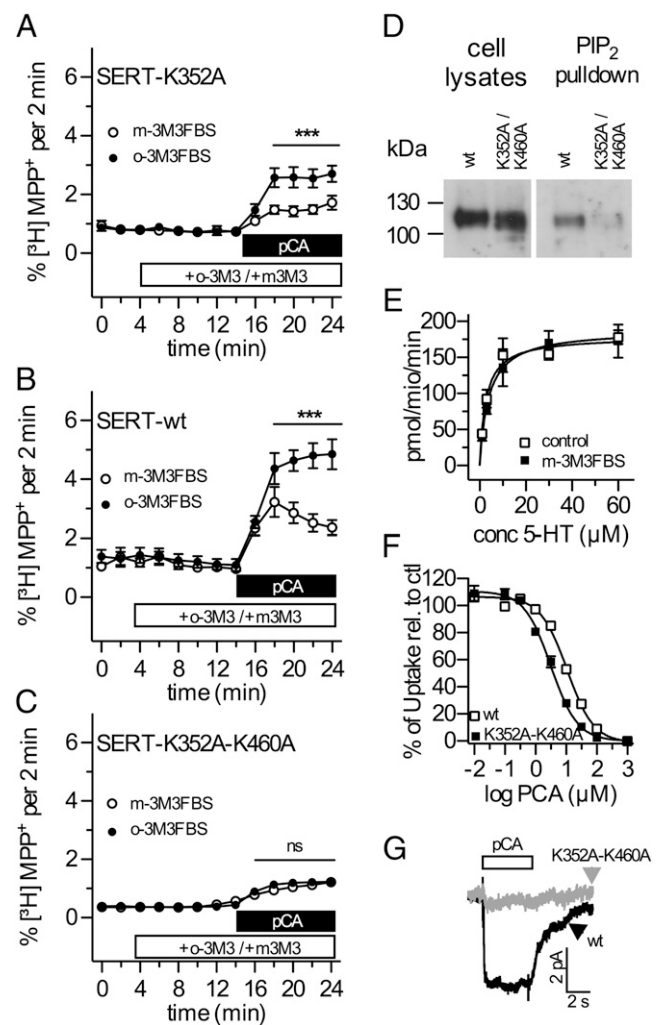
In contrast to the scattered positively charged area that covers the cytosolic side of GAT1 (Fig. 3D), roughly half the intracellular face of SERT has a positive surface potential (Fig. 3E). Here, a conspicuous patch of positively charged amino acids including residues R144 (helix 2), K352 (helix 6), and K460 (helix 9) could



attract negatively charged molecules such as PIP₂. The size of the PIP₂ headgroups (34) would perfectly fit in between these residues (10-Å distance; Fig. S4*A*). A triple mutation of these three positively charged residues to alanine is predicted to dramatically change the electrostatic potential surrounding the transporter at the center of its cytosolic side (Fig. 3*F*); the surface containing a positive potential becomes smaller in strength and in size. Furthermore, negative charged areas appear in the center of the transporter. Therefore, we hypothesized that such an amino acid exchange would reduce the attractive force for PIP₂ binding.

Mutation of the Putative PIP₂ Binding Site in SERT Eliminates Current and Efflux. Single positively charged amino acids R144, K352, and K460 were replaced by alanines. The resulting single mutants were all expressed at the cell surface (Fig. S4*B*); they also displayed

transport characteristics comparable to those of WT SERT (Table S2), and substrate efflux was inhibited by m-3M3FBS (Fig. 4*A*; Table S2). Thus, these single point mutations did not suffice to affect the interaction between PIP₂ and SERT. This result is not



surprising because up to five positively charged residues are typically involved in the binding of PIP₂ to ion channels (33). Therefore, double mutations of these residues (SERT-R144A-K352A, SERT-R144A-K460A, SERT-K352A-K460A) were generated; these also led to surface expression levels and transport rates similar to those of WT SERT (Fig. 4E; Fig. S4C; Table S3). Moreover, competition of uptake by pCA was similar in mutants and WT SERT (Fig. 4F). In contrast, in all these double mutants, pCA-induced efflux was lower than in WT SERT (Fig. 4B and C; Table S3). Nevertheless, efflux was not abolished, confirming that the conformational cycling of SERT was not entirely compromised by the mutation (Fig. 4B and C). However, PIP₂ hydrolysis triggered by m-3M3FBS affected pCA-induced efflux only in the SERT double mutants carrying the R144A mutation but not in the SERT-K352A-K460A variant (Fig. 4B; Table S3). In parallel with the marked reduction in pCA-induced substrate efflux, the SERT-K352A-K460A mutant lost its ability to (i) bind PIP₂ (Fig. 4D) and (ii) mediate pCA-evoked currents (Fig. 4G). In contrast, the double mutants that originally included R144 showed pCA-induced currents that were comparable to those through WT SERT (Fig. S4D).

This functional disparity between the three double mutants was not predicted by the electrostatic potentials shown in the model in Fig. 3E. However, estimating the distances between the mutated residues indicated that R144 is located in a very central position of SERT. This location precludes binding of PIP₂ because it simply cannot be reached from the rim of the membrane (Fig. 3E; Fig. S4A). In addition, the mutation-induced change of electrostatic forces would even add to repel PIP₂ from SERT because its central region now carries a more negative potential centered on the transporter vestibule (Fig. 3E).

As shown above, the activation of PLC either directly by m-3M3FBS or via B₂ receptors reduced currents and reverse transport through SERT. Equivalent results were obtained when potential interactions of PIP₂ with membrane proteins were prevented by interfering peptides, and direct binding between SERT and PIP₂ was demonstrated. Together, these data reveal SERT to interact with and to be functionally regulated by PIP₂.

Unlike the effects of the PIP₂ binding peptides (18), the functional consequences of PLC activation may involve not only loss of PIP₂, but also the generation of PIP₂ cleavage products, DAG and IP₃, and downstream signaling elements. Although loss of PIP₂ from the cells under investigation as a result of PLC activation

has been demonstrated, activation of PKC and increases in intracellular Ca²⁺ were evidenced not to be involved in the effects observed. Moreover, inwardly directed transport through SERT was not affected by PLC activation, thereby excluding general regulatory mechanisms such as changes in surface expression.

As previously reported for various ion channels (8), the present results reveal positively charged PIP₂ binding sites within the intracellular domains of SERT. Mutational loss of charges within these regions led to largely reduced PIP₂ binding to SERT and prevented the functional effects of PIP₂ depletion (a huge decrease in SERT-mediated currents and substrate efflux), whereas 5HT uptake and its inhibition by competitors remained unaltered. These data confirm inward and outward transport as distinct mechanistic phenomena within monoamine transporters (10, 35). Hence, altered ion flux could regulate neuronal excitability; along those lines, the studies by Carvelli et al. do in fact speak to a role for DAT currents *in vivo* (36).

A segregation of currents and reverse transport from substrate uptake has also been identified in a rare variant of the human DAT, A559V, in a pedigree of patients diagnosed with attention deficit hyperactivity disorder (37). This mutation leads to a transporter no longer showing amphetamine-induced release of monoamines, as was observed here as consequence of either PIP₂ depletion or specific amino acid exchanges. Thus, the selective interference with PIP₂ binding to SERT to prevent amphetamine-induced efflux without affecting SERT-dependent reuptake may hold therapeutic promise for amphetamine-addicted patients.

Experimental Procedures

Experimental procedures for electrophysiology and amperometry have been performed as described (15, 16, 23, 35). Biochemical assays such as pull-down assays, biochemical tracer flux analysis, and HPLC determination of pCA have been reported earlier (22–25). More detailed information on the experimental procedures including MS, confocal laser scanning microscopy, and molecular modeling, and all reagents are provided in *SI Experimental Procedures*.

ACKNOWLEDGMENTS. We gratefully acknowledge the contribution of Shimadzu (MALDI Technologies Group, Manchester, UK) for providing the MALDI instrumentation. We acknowledge financial support from FWF Grants P18706, P22893, W1232, and F35-06 (to H.H.S.), W1232 and F35-02 (to G.F.E.), and P17611 (to S.B.); National Institutes of Health Grant DA13975 (to A.G.), and a Health Research Board/Marie Curie Postdoctoral mobility fellowship (to T.M.).

1. Di Paolo G, De Camilli P (2006) Phosphoinositides in cell regulation and membrane dynamics. *Nature* 443(7112):651–657.
2. Tolias KF, Cantley LC (1999) Pathways for phosphoinositide synthesis. *Chem Phys Lipids* 98(1–2):69–77.
3. Marín-Vicente C, Nicolás FE, Gómez-Fernández JC, Corbalán-García S (2008) The PtdIns(4,5)P₂ ligand itself influences the localization of PKC α in the plasma membrane of intact living cells. *J Mol Biol* 377(4):1038–1052.
4. Pike LJ, Miller JM (1998) Cholesterol depletion delocalizes phosphatidylinositol bisphosphate and inhibits hormone-stimulated phosphatidylinositol turnover. *J Biol Chem* 273(23):22298–22304.
5. Di Paolo G, et al. (2004) Impaired PtdIns(4,5)P₂ synthesis in nerve terminals produces defects in synaptic vesicle trafficking. *Nature* 431(7007):415–422.
6. Haucke V (2005) Phosphoinositide regulation of clathrin-mediated endocytosis. *Biochem Soc Trans* 33(Pt 6):1285–1289.
7. Hilgemann DW, Ball R (1996) Regulation of cardiac Na⁺, Ca²⁺-exchange and KATP potassium channels by PIP₂. *Science* 273(80):956–959.
8. Gamper N, Shapiro MS (2007) Regulation of ion transport proteins by membrane phosphoinositides. *Nat Rev Neurosci* 8(12):921–934.
9. Kristensen AS, et al. (2011) SLC6 neurotransmitter transporters: Structure, function, and regulation. *Pharmacol Rev* 63(3):585–640.
10. Sitte HH, Freissmuth M (2010) The reverse operation of Na⁽⁺⁾/Cl⁽⁻⁾-coupled neurotransmitter transporters—why amphetamines take two to tango. *J Neurochem* 112(2):340–355.
11. Guicheney P, et al. (1988) Platelet 5-HT content and uptake in essential hypertension: Role of endogenous digitalis-like factors and plasma cholesterol. *J Hypertens* 6(11):873–879.
12. Scanlon SM, Williams DC, Schloss P (2001) Membrane cholesterol modulates serotonin transporter activity. *Biochemistry* 40(35):10507–10513.
13. Magnani F, Tate CG, Wynne S, Williams C, Haase J (2004) Partitioning of the serotonin transporter into lipid microdomains modulates transport of serotonin. *J Biol Chem* 279(37):38770–38778.
14. Hong WC, Amara SG (2010) Membrane cholesterol modulates the outward facing conformation of the dopamine transporter and alters cocaine binding. *J Biol Chem* 285(42):32616–32626.
15. Hilber B, et al. (2005) Serotonin-transporter mediated efflux: A pharmacological analysis of amphetamines and non-amphetamines. *Neuropharmacology* 49(6):811–819.
16. Hilgemann DW, Feng S, Nasuhoglu C (2001) The complex and intriguing lives of PIP₂ with ion channels and transporters. *Sci STKE* 2001(111):re19.
17. Schicker K, et al. (2012) Unifying concept of serotonin transporter-associated currents. *J Biol Chem* 287(1):438–445.
18. Robbins J, Marsh SJ, Brown DA (2006) Probing the regulation of M (Kv7) potassium channels in intact neurons with membrane-targeted peptides. *J Neurosci* 26(30):7950–7961.
19. Bae Y-S, et al. (2003) Identification of a compound that directly stimulates phospholipase C activity. *Mol Pharmacol* 63(5):1043–1050.
20. Mager S, et al. (1994) Conducting states of a mammalian serotonin transporter. *Neuron* 12(4):845–859.
21. Gutowski S, et al. (1991) Antibodies to the alpha q subfamily of guanine nucleotide-binding regulatory protein alpha subunits attenuate activation of phosphatidylinositol 4,5-bisphosphate hydrolysis by hormones. *J Biol Chem* 266(30):20519–20524.
22. Quick MW (2003) Regulating the conducting states of a mammalian serotonin transporter. *Neuron* 40(3):537–549.
23. Sitte HH, et al. (1998) Carrier-mediated release, transport rates, and charge transfer induced by amphetamine, tyramine, and dopamine in mammalian cells transfected with the human dopamine transporter. *J Neurochem* 71(3):1289–1297.
24. Khoshbouei H, Wang H, Lechleiter JD, Javitch JA, Galli A (2003) Amphetamine-induced dopamine efflux. A voltage-sensitive and intracellular Na⁺-dependent mechanism. *J Biol Chem* 278(14):12070–12077.

25. Seidel S, et al. (2005) Amphetamines take two to tango: An oligomer-based counter-transport model of neurotransmitter transport explores the amphetamine action. *Mol Pharmacol* 67(1):140–151.
26. Sitte HH, et al. (2001) Quantitative analysis of inward and outward transport rates in cells stably expressing the cloned human serotonin transporter: Inconsistencies with the hypothesis of facilitated exchange diffusion. *Mol Pharmacol* 59(5): 1129–1137.
27. Várnai P, Balla T (1998) Visualization of phosphoinositides that bind pleckstrin homology domains: Calcium- and agonist-induced dynamic changes and relationship to myo-[3H] inositol-labeled phosphoinositide pools. *J Cell Biol* 143(2):501–510.
28. Johnson LA, Guptaroy B, Lund D, Shamban S, Gney ME (2005) Regulation of amphetamine-stimulated dopamine efflux by protein kinase C beta. *J Biol Chem* 280(12): 10914–10919.
29. Gney ME, et al. (2004) Intracellular Ca²⁺ regulates amphetamine-induced dopamine efflux and currents mediated by the human dopamine transporter. *Mol Pharmacol* 66(1):137–143.
30. Schmitt KC, Reith MEA (2010) Regulation of the dopamine transporter: Aspects relevant to psychostimulant drugs of abuse. *Ann N Y Acad Sci* 1187:316–340.
31. Nelson N (1998) The family of Na⁺/Cl⁻ neurotransmitter transporters. *J Neurochem* 71(5):1785–1803.
32. Beuming T, Shi L, Javitch JA, Weinstein H (2006) A comprehensive structure-based alignment of prokaryotic and eukaryotic neurotransmitter/Na⁺ symporters (NSS) aids in the use of the LeuT structure to probe NSS structure and function. *Mol Pharmacol* 70(5):1630–1642.
33. Rosenhouse-Dantsker A, Logothetis DE (2007) Molecular characteristics of phosphoinositide binding. *Pflügers Archiv* 455(1):45–53.
34. Haider S, Tarasov AI, Craig TJ, Sansom MSP, Ashcroft FM (2007) Identification of the PIP2-binding site on Kir6.2 by molecular modelling and functional analysis. *EMBO J* 26(16):3749–3759.
35. Robertson SD, Matthies HJG, Galli A (2009) A closer look at amphetamine-induced reverse transport and trafficking of the dopamine and norepinephrine transporters. *Mol Neurobiol* 39(2):73–80.
36. Carvelli L, et al. (2004) Dopamine transporters depolarize neurons by a channel mechanism. *Proc Natl Acad Sci USA* 101(45):16046–16051.
37. Mazei-Robison MS, et al. (2008) Anomalous dopamine release associated with a human dopamine transporter coding variant. *J Neurosci* 28(28):7040–7046.

Supporting Information

Buchmayer et al. 10.1073/pnas.1220552110

SI Experimental Procedures

Reagents. The following lipid standards were purchased from Avanti Polar Lipids: 1-heptadecanoyl-2-(9Z-tetradecenoyl)-sn-glycero-3-phospho-(1'-myo-inositol) (17:0–14:1 PI; $M_w = 794.49$), 1-heptadecanoyl-2-(5Z,8Z,11Z,14Z-eicosatetraenoyl)-sn-glycero-3-phospho-(1'-myo-inositol-3'-phosphate) (17:0–20:4 PI(3)P; $M_w = 952.51$), 1-heptadecanoyl-2-(5Z,8Z,11Z,14Z-eicosatetraenoyl)-sn-glycero-3-phospho-(1'-myo-inositol-3',5'-bisphosphate) (17:0–20:4 PI(3,5)P₂; $M_w = 1032.47$), and 1-heptadecanoyl-2-(5Z,8Z,11Z,14Z-eicosatetraenoyl)-sn-glycero-3-phospho-(1'-myo-inositol-3',4',5'-trisphosphate) (17:0–20:4 PI(3,4,5)P₃; $M_w = 1112.44$). 6-Aza-2-thiothymine (ATT), chloroform (CHCl₃), hydrochloric acid (HCl), and phorbol-12-myristate-13-acetate (β -PMA) were purchased from Sigma-Aldrich. Dibasic ammonium citrate [diammonium hydrogen citrate (DAHC)] was purchased from Fluka. Ethanol (EtOH), methanol (MeOH), and ultrapure water (UHQ) were obtained from Merck. Bradykinin was from Fluka/Sigma-Aldrich; Hoe 140, phenyl-arseneoxide (PAO), m-3M3FBS {2,4,6-trimethyl-N-[3-(trifluoromethyl)phenyl]benzenesulfonamide}, GF109203X, GABA, 5HT, methyl-phenylpyridinium (MPP⁺), and DL-*para*-chloroamphetamine-HCl (pCA) were from Sigma-Aldrich. o-3M3FBS and U73122 were from Tocris. BAPTA/AM was from VWR International. The small peptide pal-HRQKHFEKRR (90–95% purity, HPLC grade) was purchased from ³iChem and dissolved in DMSO (analytical grade). Tritiated MPP⁺ was purchased from American Radiolabeled Chemicals, and tritiated GABA and 5HT were from PerkinElmer. Phosphatidylinositol-4,5-bisphosphate (PIP₂)-coated beads were obtained from Echelon. Anti-GFP antibody was purchased from Invitrogen. All other chemicals and standard reagents were obtained from different commercial sources in the highest purity grade available.

PIP₂ Pull-Down Assay and Immunoblotting. Human embryonic kidney 293 (HEK) cells stably expressing the YFP-tagged SERT or parental HEK cells were solubilized in lysis buffer containing 0.9% Triton X-100, 20 mM Tris-HCl (pH 8.0), 150 mM NaCl, 1 mM EDTA, 5 mM sodium fluoride, and a protease inhibitor mixture (complete; Roche) on a tube rotator for 30 min at 4 °C. After centrifugation at 14,000 × g for 10 min at 4 °C, the supernatant was collected and incubated overnight with either PIP₂ beads or control beads at 4 °C. After six times washing with lysis buffer, bound proteins to PIP₂ beads were eluted in 2× SDS loading buffer [125 mM Tris-HCl, 20% (vol/vol) glycerol, 4% (wt/vol) SDS, 10% (vol/vol) 2-mercaptoethanol, 0.02% bromophenol blue, pH 6.8] at 95 °C for 3 min. Cell lysates and eluents were resolved on 10% (wt/vol) SDS polyacrylamide gels and transferred to PVDF for immunoblotting with an anti-GFP antibody.

Electrophysiology. For patch-clamp recordings, HEK cells stably (1) or transiently expressing serotonin transporter [human SERT (hSERT)] were seeded at low density for 24 h before the measurement. Substrate-induced SERT-mediated currents were determined as described in detail elsewhere (2). In brief, cells were voltage clamped using the whole cell variant. Electrodes were filled with a solution consisting of (mM) 133 potassium gluconate, 5.9 NaCl, 1 CaCl₂, 0.7 MgCl₂, 10 Hepes, and 10 EGTA, adjusted to pH 7.2 with KOH. Cells were superfused with a solution containing (mM) 140 NaCl, 3 KCl, 2.5 CaCl₂, 2 MgCl₂, 10 Hepes, and 20 glucose, adjusted to pH 7.4 with NaOH.

Currents were recorded at room temperature using an Axopatch 200B amplifier and pClamp 10.2 software (MDS Analytical Technologies). Cells were voltage clamped to a holding potential of –70 mV. Either pCA or 5HT were applied thrice for 4 s, each application followed by a 60 s wash period. Subsequently, drug was applied for 10 min and a second sequence of substrate application. Current traces were filtered at 1 kHz and digitized at 2 kHz using Digidata 1320A (MDS Analytical Technologies). Liquid junction potential was calculated to be 16 mV and was compensated. Drugs were applied using a DAD-12 system (Adams and List), which permits complete solution exchange around the cells within 100 ms (3). Current amplitudes in response to substrate application were quantified using Clampfit 10.2. Passive holding currents were subtracted, and the traces were filtered using a 100-Hz digital Gaussian low-pass filter.

Amperometry. HEK cells stably expressing hSERT [hS4TO (1)] were plated at a density of ~10³ per 35-mm culture dish. To load cells with 5HT and either scrambled peptide or pal-HRQKHFEKRR, a programmable puller (model P-2000; Sutter Instruments) was used to fabricate quartz recording pipettes with a resistance of 5 MΩ. The pipettes were filled with a peptide- and 5HT-containing internal solution (120 mM KCl, 10 mM Hepes, 0.1 mM CaCl₂, 2 mM MgCl₂, 1.1 mM EGTA, 30 mM dextrose, pH 7.35, and 275 mOSM; plus 2 mM 5HT and 10 μM scrambled peptide or pal-HRQKHFEKRR). The dishes were washed with the external bath solution (130 mM NaCl, 10 mM Hepes, 34 mM D-glucose, 1.5 mM CaCl₂, 0.5 mM MgSO₄, 1.3 mM KH₂PO₄, adjusted pH to 7.35, and 300 mOsm). On gaining access to the cells, the 5HT- and peptide-containing internal solution was allowed to diffuse into the cell for 10 min. A carbon fiber electrode (ProCFE; fiber diameter of 5 μm; obtained from Dagan Corporation) juxtaposed to the plasma membrane and held at +700 mV (a potential greater than the oxidation potential of 5HT) was used to measure 5HT flux through oxidation reactions. Cells were not voltage clamped to permit measurement of basal efflux under resting membrane potential conditions. Amperometric currents in response to an addition of 10 μM D-amphetamine were recorded using an Axopatch 200B amplifier (Molecular Devices) with a low-pass Bessel filter set at 1 kHz; traces were digitally filtered offline at 1 Hz using Clampex9 software (Molecular Devices).

Lipid Extraction. A two-step organic solvent extraction protocol modified after the literature (4) was used to separate phosphatidylinositol (PI) and PIPs. Briefly, 500 μL ice-cold CHCl₃:MeOH = 50:50 (vol/vol) was added to the cell pellet (~10⁶ cells), vigorously vortexed for about 1–2 min, and centrifuged for 5 min (3,381 × g). Afterward, the supernatant containing the majority of PIs [>95% (vol/vol)] was collected into glass vials (=extract 1), and the cell pellet was extracted again by adding 200 μL CHCl₃:MeOH = 70:30 (vol/vol, containing 0.3% aqueous HCl), sonicated for 15–30 s to homogenize the cell pellet, and vortexed vigorously for 5 min. Fifty microliters 1 N HCl dissolved in UHQ was added, vortexed shortly for 1–2 min, and centrifuged for 5 min (3,381 × g) to separate into an aqueous upper and organic lower phase. Finally, the organic phase containing the majority of PIPs (>98%) was collected and transferred to glass vials (=extract 2).

MALDI Sample Preparation. For the MALDI sample preparation, FlexiMass-DS disposable polymeric slides (Shimadzu) and 6-aza-2-thiothymine (ATT) matrix dissolved in EtOH:H₂O = 90:10 containing 10 mM DAHC as additive were used (5). Quantification of

PIPs was accomplished using LIPID MAPS approved PIP standards (ISDs) containing nonnaturally occurring fatty acid residues. Generally, the sample and PIP standard mixture containing 3 pmol/ μ L each were mixed before analysis, and 1 μ L of the mixture was spotted onto the MALDI target. This procedure provided the best mass spectral quality for structure verification by MALDI-MS/MS analysis and signal reproducibility for quantitative measurements.

MALDI MS. MALDI-TOF mass spectra were acquired on an AXIMA-CFR^{plus} instrument (Shimadzu) equipped with a curved-field reflectron and a nitrogen laser ($\lambda = 337$ nm). MALDI-MS/MS spectra for identification of individual PIP molecular species were acquired by a hybrid MALDI-QIT-TOF-MS instrument (AXIMA-Resonance; Shimadzu) using collision-induced dissociation (CID) experiments, whereby argon was used as collision gas. All measurements were performed in the negative ion mode using delayed ion extraction for baseline monoisotopic mass resolution over the whole mass range under observation (m/z 200–2,000). Each MALDI mass spectrum shown represents the accumulation of 300–500 single laser shots. An internal mass calibration using exact m/z values of the [M-H]⁻ ions of the lipid standards indicated above was performed. MALDI data processing was performed by the manufacturer supplied instrument software versions Launchpad 2.8 (AXIMA-CFR^{plus}) and 2.9.1 (AXIMA-Resonance), using the Savitzky-Golay smoothing algorithm.

PIP Quantification. Based on MALDI-MS analysis of PIP standards, a linear detection over three orders of magnitude (LOD \sim 0.06 pmol/ μ L) spanning the PI(P) concentration range within the samples was obtained. For quantification of PIPs, cell extracts 1 and 2 were measured independently to determine the signal intensity ratio of PIs and PIPs to their corresponding ISDs. These ratios were used to determine the individual amount of PIPs (measured in extract 2) displayed as percentage of the corresponding PI precursor species (measured in extract 1).

Uptake and Release Assays. Uptake experiments were performed as described (1). In brief, for the determination of nonspecific uptake, we used 10 μ M paroxetine (preincubation time, 5 min), and 0.1 μ M [³H]5HT was added for 3 or 1 min, respectively; for GAT1, 0.2 μ M [³H]GABA was added for 3 min, and 10 μ M tiagabine was used for the determination of nonspecific uptake (preincubation time, 3 min). Before the experiment, the cells were washed once in uptake buffer [in mM: Hepes (25), NaCl (120), KCl (5), CaCl₂ (1.2), and MgSO₄ (1.2) supplemented with D-glucose (5)] and equilibrated in uptake buffer for 10 min before starting the assay. Nonlabeled substrate was added at increasing concentrations as indicated to a final volume of 100 μ L. After incubation for 1 or 3 min at room temperature, cells were washed in ice-cold uptake buffer, and the remaining radioactivity was determined by liquid scintillation counting. *o*-3M3FBS, *m*-3M3FBS, or PAO was preincubated for 10 min in the concentrations indicated in the figure legends.

Substrate efflux assays in heterologous cell systems and rat striatal slices were performed as previously described (6). In brief, culture medium was removed from stably or transiently transfected HEK cells (4×10^5 cells per well grown on coverslips in 96-well plates) or striatal slices, and the cells/slices were preincubated with 0.1 μ M [³H]MPP⁺ or [³H]GABA for 20 min at 37 °C in a final volume of 0.1 mL Krebs-Ringer-Hepes buffer (KHB) per well. The coverslips/slices were transferred into chambers, and excess radioactivity was subsequently washed out with buffer at 25 °C for 45 min at a perfusion rate of 0.7 mL/min. Once stable efflux of radioactivity was achieved, following the initial wash, 2-min fractions were collected, and samples were counted in a beta counter.

Homology Modeling and Electrostatic Surface Potential. The homology model of SERT was created based on the bacterial amino acid transporter LeuT, using the sequence alignment of ref. 7 and including structural information like a disulfide bond in EL-2 between C200 and C209. The model of the triple alanine mutant was created by introducing the three mutations R144A, K352A, and K460A. The homology model of GAT1 was created using the SERT model as a template. We could therefore create a consistent set of models, where similar side chains are oriented in a similar way. Consistent side chain orientation is especially important for surface exposed, flexible, and charged side chains, as the details of their orientation will influence the potential iso-surface.

To analyze the electrostatic potential, we assigned Amber 99 (8) type charges to the homology models using the program pdb2pqr (9). Subsequently the Poisson-Boltzmann equation was solved using the adaptive Poisson-Boltzmann solver (APBS) (10). The electrostatic interactions were evaluated assuming a salt concentration of 0.15 mM and a temperature of 37 °C. The electrostatic potential was visualized using the graphics program Visual Molecular Dynamics (VMD) by displaying an iso-surface of the potential. A membrane surrounding was added for visualization and orientation purposes.

Mutagenesis. Mutations to SERT were introduced using the Quickchange Lightning Kit (Agilent). Primers used were as follows: R144A, GCACTGGGACAGTACACGCAAAT-GGTTGCATTCAATATGGAGG; K352A, TGGCTTTTG-CTAGCTACAACCGCGTTCAACAACAACTGCTACC; and K460A, GTTCCCACACGTCTGCGCAGCGGCCGGGA-GCGGTT.

Confocal Laser Scanning Microscopy. Life cell imaging was performed as previously described (11). In brief, HEK cells either transfected or stably expressing YFP-SERT WT or mutant forms thereof were grown on 15-mm coverslips in DMEM plus 10% (vol/vol) FCS. Cells were preincubated with the fluorescent rhodamine cocaine analog JHC1-64 and dissolved in PBS (plus 5 mM glucose) for 20 min at room temperature before the addition of either 25 μ M *m*-3M3FBS or 25 μ M *o*-3M3FBS for 20 min at room temperature. Live cell imaging was performed using a Zeiss LSM 510 confocal microscope, equipped with an Argon laser (30 mW) and a helium-neon laser (1 mW), and a 63 \times oil immersion Zeiss Plan-Neofluar 1.4 objective. JHC1-64 was visualized using a 543-nm HeNe laser line and a 585-nm long-pass filter. YFP was visualized using a 514-nm argon laser and a 505- to 530-nm band-pass filter at 30–45% input power.

The thickness of the optical sections was between 0.8 and 1.5 μ m (frame scan) at 30–45% input power.

Cell Surface Biotinylation. Cells were seeded into poly-D-lysine-coated six-well plates. The next day, cells were washed with KHB before incubation with *m*-3M3FBS, *o*-3M3FBS (25 μ M each), PMA (1 μ M), or DMSO for 20 min at room temperature. WT and mutant SERT were serum-starved for 2.5 h. After preincubation, cells were washed three times with ice-cold PBS²⁺ (PBS with 1 mM MgCl₂, 0.1 mM CaCl₂) before incubation with sulfo-NHS-SS-biotin (1 mg/mL) in KHB for 15 min at 4 °C. The incubation was quenched with 100 mM glycine in KHB. Cells were finally lysed in lysis buffer [10 mM Tris-HCl, pH = 7.4, 150 mM NaCl, 1 mM EDTA, 1% (vol/vol) Triton X-100, 0.1% SDS] supplemented with protease inhibitor mixture (Roche complete). The lysates were incubated with streptavidin beads overnight at 4 °C. The next day, beads were washed three times with lysis buffer and subjected to SDS/PAGE. After electrotransfer membranes were blocked with 5% (wt/vol) BSA for 1 h at room temperature before incubation with primary antibodies (rabbit anti-GFP, 1:10,000; mouse

anti-tubulin, 1:20,000) overnight. The next day, membranes were washed with Tris-buffered saline + 0.1% Tween-20 and incubated with secondary antibodies. Immunoreactive bands were detected using the enhanced chemiluminescence method, and band densities were quantified by ImageJ.

- Hilber B, et al. (2005) Serotonin-transporter mediated efflux: A pharmacological analysis of amphetamines and non-amphetamines. *Neuropharmacology* 49(6):811–819.
- Schicker K, et al. (2012) Unifying concept of serotonin transporter-associated currents. *J Biol Chem* 287(1):438–445.
- Boehm S (1999) Presynaptic alpha2-adrenoceptors control excitatory, but not inhibitory, transmission at rat hippocampal synapses. *J Physiol* 519(Pt 2):439–449.
- Kim Y, Shanta SR, Zhou L-H, Kim KP (2010) Mass spectrometry based cellular phosphoinositides profiling and phospholipid analysis: A brief review. *Exp Mol Med* 42(1):1–11.
- Stübiger G, et al. (2010) Analysis of oxidized phospholipids by MALDI mass spectrometry using 6-aza-2-thiothymine together with matrix additives and disposable target surfaces. *Anal Chem* 82(13):5502–5510.
- Scholze P, et al. (2002) The role of zinc ions in reverse transport mediated by monoamine transporters. *J Biol Chem* 277(24):21505–21513.
- Beuming T, Shi L, Javitch JA, Weinstein H (2006) A comprehensive structure-based alignment of prokaryotic and eukaryotic neurotransmitter/ Na^+ symporters (NSS) aids in the use of the LeuT structure to probe NSS structure and function. *Mol Pharmacol* 70(5):1630–1642.
- Wang J, Cieplak P, Kollman PA (2000) How well does a restrained electrostatic potential (RESP) model perform in calculating conformational energies of organic and biological molecules? *J Comput Chem* 21:1049–1074.
- Dolinsky TJ, Nielsen JE, McCammon JA, Baker NA (2004) PDB2PQR: An automated pipeline for the setup of Poisson-Boltzmann electrostatics calculations. *Nucleic Acids Res* 32(Web Server issue):W665–7.
- Baker NA, Sept D, Joseph S, Holst MJ, McCammon JA (2001) Electrostatics of nanosystems: Application to microtubules and the ribosome. *Proc Natl Acad Sci USA* 98(18):10037–10041.
- Eriksen J, et al. (2009) Visualization of dopamine transporter trafficking in live neurons by use of fluorescent cocaine analogs. *J Neurosci* 29(21):6794–6808.

Table S1. Comparison of MPP⁺ uptake by SERT expressing HEK cells with and without PIP2 depletion

| MPP ⁺ uptake | hSERT WT | | |
|--------------------------|--------------|------------------|------------------|
| | Control | <i>m</i> -3M3FBS | <i>o</i> -3M3FBS |
| $V_{\max} \pm \text{SE}$ | 450.7 ± 30.6 | 413.5 ± 20.3 | 458.9 ± 25.3 |
| $K_m \pm \text{SE}$ | 8.5 ± 1.5 | 7.0 ± 1.0 | 7.9 ± 1.2 |

All experiments were performed four times in triplicate. Uptake of MPP⁺ in the presence of *m*-3M3FBS (25 μM) or *o*-3M3FBS (25 μM) or buffer (control). V_{\max} values are expressed as pmol/min/ 10^6 cells and K_m values in μM . Stably transfected cells expressed hSERT under the control of a tetracycline-dependent repressor as described in *Experimental Procedures* and published earlier (1).

- Hilber B, et al. (2005) Serotonin-transporter mediated efflux: a pharmacological analysis of amphetamines and non-amphetamines. *Neuropharmacology* 49(6):811–819.

Table S2. Effect of PIP2 depletion on the uptake and efflux of MPP⁺ in HEK cells expressing either wt or single mutants of SERT

| hSERT | MPP ⁺ uptake | | [³ H]-MPP ⁺ efflux (% ± SE) | |
|-------|--------------------------|------------------------|--|------------------------|
| | $V_{\max} \pm \text{SE}$ | $K_m \pm \text{SE}$ | <i>o</i> -3M3FBS | <i>m</i> -3M3FBS |
| WT | 25.6 ± 3.2* | 5.0 ± 2.0* | 3.3 ± 0.3 [†] | 1.5 ± 0.3 [†] |
| R144A | 43.8 ± 5.6 [†] | 4.9 ± 1.9 [†] | 4.0 ± 0.2 [‡] | 1.9 ± 0.1 [‡] |
| K352A | 15.5 ± 1.5 [†] | 6.8 ± 2.5 [†] | 1.8 ± 0.2 [‡] | 0.7 ± 0.1 [‡] |
| K460A | 22.8 ± 1.4 [†] | 1.3 ± 0.6 [†] | 5.8 ± 0.2 [‡] | 1.7 ± 0.3 [‡] |

Series of uptake and efflux experiments using MPP⁺ in cells transiently expressing single hSERT mutants tagged with YFP to monitor expression (CaPO₄ transfection method). V_{\max} values are expressed as pmol/min/ 10^6 cells and K_m values in μM (all experiments were performed in triplicate determination). Efflux values are expressed in percent per 2 min in the presence of *m*-3M3FBS (25 μM) or *o*-3M3FBS (25 μM ; all experiments were performed in triplicate determination).

* $n = 4$.

[†] $n = 3$.

[‡] $n = 7$.

^{*} $n = 3$ –6.

Table S3. Effect of PIP₂ depletion on the uptake and efflux of MPP⁺ in HEK cells expressing either wt or double mutants of SERT

| hSERT | MPP ⁺ uptake | | [³ H]-MPP ⁺ efflux (% \pm SE) | |
|-------------|-------------------------------|----------------------------|--|-----------------------------|
| | V _{max} \pm SE | K _m \pm SE | o-3M3FBS | m-3M3FBS |
| WT | 268.3 \pm 15.8* | 4.6 \pm 0.5* | 3.3 \pm 0.3 [†] | 1.5 \pm 0.3 [†] |
| K352A/K460A | 222.5 \pm 18.4 [†] | 4.1 \pm 1.0 [†] | 0.8 \pm 0.1 [¶] | 0.7 \pm 0.04 [¶] |
| K352A/R144A | 122.0 \pm 7.1 [†] | 2.3 \pm 0.6 [†] | 0.6 \pm 0.1 [¶] | 0.25 \pm 0.1 [¶] |
| K460A/R144A | 291.6 \pm 21.1 [†] | 2.9 \pm 0.9 [†] | 0.9 \pm 0.1 [¶] | 0.5 \pm 0.1 [¶] |

Series of uptake and efflux experiments using MPP⁺ in cells transiently expressing hSERT double mutants tagged with YFP to visualize expression (lipofection). V_{max} values are expressed as pmol/min/mio cells and K_m values in μ M (all experiments were performed in triplicate determination). Efflux values are expressed in percent per 2 min in the presence of m-3M3FBS (25 μ M) or o-3M3FBS (25 μ M; all experiments were performed in triplicate determination).

*n = 3.

[†]n = 9.

[¶]n = 11.

^{*}n = 3–6.

Fig. S1. (A) Determination of the PIP₂ content in HEK-SERT cells (Left). The m/z values of PIP₂ were calculated from the major PI species detected by MALDI-MS in HEK-SERT cells: three major PIP (m/z 915, 941, 967) and PIP₂ (m/z 995, 1021, 1047) species were detected, respectively. A molecular structural analysis using MALDI-quadrupole-ion-trap-TOF-MS/MS was performed to confirm the identity of these PIPs. According to that, the PIP₂ species were identified as 1-palmitoyl-2-oleoyl-sn-glycero-3-phospho-inositol-4',5'-bisphosphate (34:1-PIP₂; m/z 995), 1,2-dioleoyl-sn-glycero-3-phospho-inositol-4',5'-bisphosphate (36:2-PIP₂; m/z 1021), and 1-stearoyl-2-eicosatrienoyl-sn-glycero-3-phospho-inositol-4',5'-bisphosphate (38:3-PIP₂; m/z 1049). Following that, the amount of the PIP₂ species relative to an internal standard (m/z 1031) was calculated to measure the effects of m-3M3FBS and o-3M3FBS on PIP₂ expression, respectively. Representative MALDI mass spectra indicating the m/z values from peaks corresponding to PIPs are shown. The signals at m/z 995.47, 1,021.45, and 1,047.47 correspond to the major PIP₂ molecular species detected from HEK-SERT cells. The peak at m/z 1,031 (indicated by the solid arrow) represents the PIP₂ internal standard used. Summary of the PIP₂ content in HEK-SERT cells (Right). Mean results from MALDI-TOF-MS analysis of the cells treated with o-3M3FBS and m-3M3FBS, respectively. Signals at m/z 995.47, 1021.45, and 1,047.47 corresponded to the major PIP₂ molecular species detected. Arithmetic means (\pm SEM) of semiquantitative analyses of the PIP₂ species from the MALDI mass spectra of three independent experiments are shown (black: o-3M3FBS; white: m-3M3FBS). Significance was tested by one-way ANOVA followed by Bonferroni's post hoc test (**P < 0.01). (B) Current traces from single HEK HEK-SERT cells coexpressing B₂ bradykinin receptors: application of pCA (3 μ M) is indicated by the bar. Traces were obtained in the presence and absence of either 10 nM bradykinin or 10 nM bradykinin and Hoe140 as indicated.

Fig. S1

Fig. S2. (A) Confocal laser scanning microscopy images of GFP-tagged PKC- β II transiently expressed in HEK cells. Cells were seeded onto glass coverslips and images were captured as outlined in SI Experimental Procedures. The images are representative of seven (m-3M3FBS; 25 μ M) and eight images (o-3M3FBS; 25 μ M) captured in parallel from the same transfection. The experiment was repeated three times with independent transfections. (Upper Left) Cells were stimulated either with m-3M3FBS or with o-3M3FBS and time dependence was recorded. (Upper Right) Fluorescence profile that indicates the distribution of the fluorescence over the cell in the indicated open rectangle (black line at time point = 0 min; gray line at time point = 2 min). Intensity of F_{CYT} and F_{PM} were identified and measured in arbitrary units within a region of interest. F_{CYT} and F_{PM} values were calculated as F_{CYT} or F_{PM} intensity divided by the mean of the region of interest (ROI) for normalization between cells. The bar graph represents the mean value of all images (n = 7–8). Statistical significance was determined by one-way ANOVA with Bonferroni's post hoc test: ***P < 0.001, ns, not significant. (B) Time course of pCA-induced, SERT-mediated efflux of [³H]MPP⁺ from HEK-SERT cells. The cells were loaded with 0.1 μ M [³H]MPP⁺ and superfused, and 2-min fractions were collected. The different substances were added to the superfusion buffer as indicated. At minute 14, pCA (3 μ M) was added to induce efflux. The superfusion experiment was carried out in the presence or absence of the PKC inhibitor GF109203X (1 μ M); m-3M3FBS or o-3M3FBS were present (25 μ M), and DMSO was used in an equivalent volume for control purposes. The graph shows the mean data from three superfusion experiments performed in triplicate (n = 6–9). Statistical significance was tested using two-way ANOVA with Bonferroni's post hoc test: ***P < 0.001; ns, not significant. (C) Mean data from three to four superfusion experiments using BAPTA-AM (50 μ M) in comparison with control and in the presence or absence of m-3M3FBS (25 μ M). The data were baseline corrected, and all experiments were performed in triplicate as described in B. Statistical analysis was performed using one-way ANOVA followed by Bonferroni's post hoc test (ns, not significant). (D) (Upper) Representative confocal microscopy images of a time course examining CFP-SERT-expressing cells in the presence of m-3M3FBS or o-3M3FBS (25 μ M). Fluorescence histograms were applied at the indicated lines to examine the fluorescence ratio between transporters located in the cytosol (F_{CYT}) or at the cell surface (F_{PM}, as shown in A). Two to three cells were examined per wide field (eight images taken out of three independent transfections), and the resulting ratios were plotted against time (Lower). Please refer to SI Experimental Procedures and A for further details. (E) Cell surface levels of YFP-SERT WT were quantified by cell surface biotinylation. (Upper) Western blot analysis representative of four blots after the cells had been treated with o-3M3FBS and m-3M3FBS as indicated (25 μ M each). (Lower) Bar graph represents means \pm SEM from four independent experiments performed in triplicate; significance between the different treatments was not achieved (Mann-Whitney nonparametric test, two-tailed). Surface biotinylation experiments were carried out as described in SI Experimental Procedures. (F) Cell surface levels of YFP-SERT WT after treatment with a phorbol ester, β -PMA, were determined by uptake and cell surface biotinylation. (Upper) Western blot analysis representative of three blots after the cells had been treated with β -PMA (1 μ M) for 30 min as indicated. (Lower) Bar graph represents means \pm SEM from three independent experiments performed in triplicate; significance was observed at P < 0.05 and indicated by * (Mann-Whitney nonparametric test, two-tailed). Surface biotinylation experiments were carried out as described in SI Experimental Procedures. (Lower) Saturation curve of 5HT uptake in HEK-SERT cells in the presence or absence of 1 μ M β -PMA. The cells were plated in 48-well dishes, washed 1x with KHB, and preincubated with or without 1 μ M β -PMA for 30 min at 37 °C. Uptake was initiated by the addition of 0.1 μ Ci ³H-5HT for 1 min. Subsequently, the incubation buffer was removed and replaced with ice-cold buffer to stop the reaction. The cells were washed 2x with KHB and lysed with 1% (wt/vol) SDS. The radioactivity was determined by liquid scintillation counting. Symbols represent the mean \pm SEM of four experiments performed in triplicate.

Fig. S2

Fig. S3. Determination of PIP₂ content in HEK-GABA transporter (GAT) cells. Representative MALDI mass spectra indicating the *m/z* values from peaks corresponding to PIPs are shown. The signals at *m/z* 995.48, 1,023.15, and 1,049.53 correspond to the major PIP₂ molecular species detected from HEK-SERT cells. The peak at *m/z* 1,031 (indicated by the solid arrow) represents the PIP₂ internal standard used.

Fig. S3

Fig. S4. (A) Distance estimation within the positively charged patch consisting of R144, K352, and K460. The LeuT-based SERT homology model (1) shows distances (in Angstroms) between putative interaction partners for the negatively charged PIP₂ headgroups. The model was generated with the PRIME software module of Schrodinger, Suite 2012: Prime, version 3.1 (Schrödinger) (2, 3), and the figure was prepared using MOE (Chemical Computing Group, Inc.). (B) Confocal laser scanning microscopy images of YFP-tagged SERT WT and single amino acid mutants transiently expressed in HEK cells. Cells were seeded onto poly-D-lysine-coated glass coverslips, and images were captured as outlined in *SI Experimental Procedures*. Cells were preincubated with 20 nM JHC1-64 for 20 min at room temperature; subsequently, JHC1-64 was visualized using a 543-nm HeNe laser line and a 585-nm long-pass filter, and YFP was visualized using a 514-nm argon laser and a 505- to 530-nm band-pass filter. The experiment was repeated three times with independent transfections. (Right) Fluorescence profile that indicates the distribution of the fluorescence over the cell in the indicated open rectangle. (C) Confocal laser scanning microscopy images of YFP-tagged SERT WT and single amino acid mutants transiently expressed in HEK cells. Cells were seeded onto glass coverslips, and images were captured as outlined in *SI Experimental Procedures*. Cells were preincubated with 20 nM JHC1-64 for 20 min at room temperature; subsequently, JHC1-64 was visualized using a 543-nm HeNe laser line and a 585-nm long-pass filter, and YFP was visualized using a 514-nm argon laser and a 505- to 530-nm band-pass filter. The experiment was repeated three times with independent transfections. (D) Current traces from single HEK-SERT cells. Comparison of currents induced by application of pCA (3 μM; indicated by the bar) in HEK-SERT WT cells (black) and HEK-SERT-R144A-K460A cells (Left, gray) and HEK-SERT-R144A-K352A cells (Right, gray).

Fig. S4

1. Sarker S, et al. (2010) The high-affinity binding site for tricyclic antidepressants resides in the outer vestibule of the serotonin transporter. *Mol Pharmacol* 78(6):1026–1035.
2. Jacobson MP, Friesner RA, Xiang Z, Honig B (2002) On the role of the crystal environment in determining protein side-chain conformations. *J Mol Biol* 320(3):597–608.
3. Jacobson MP, et al. (2004) A hierarchical approach to all-atom protein loop prediction. *Proteins* 55(2):351–367.

Figure S1A:

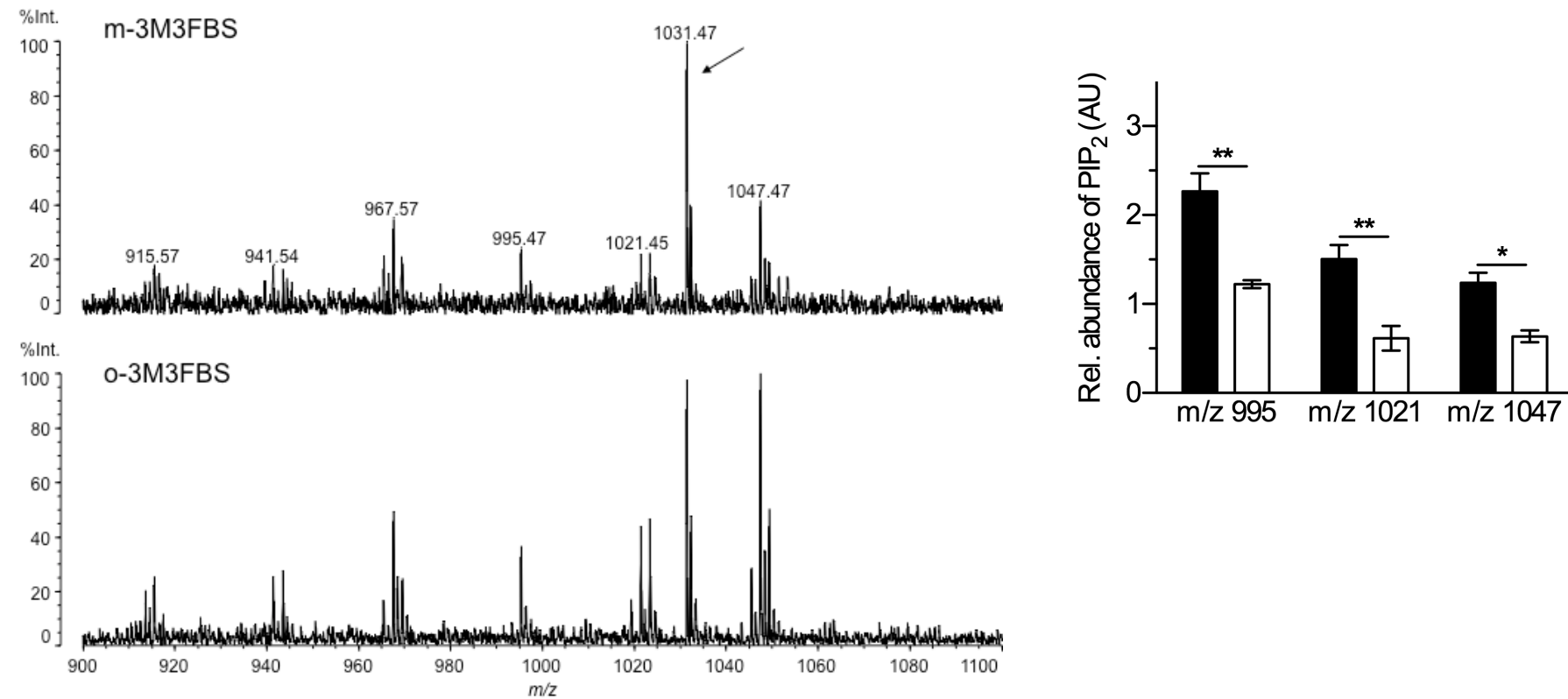


Figure S1B:

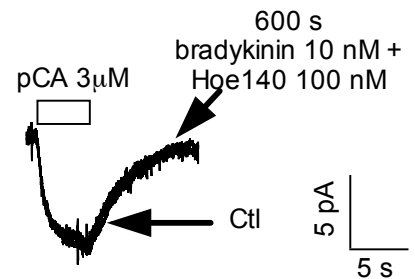


Figure S2A:

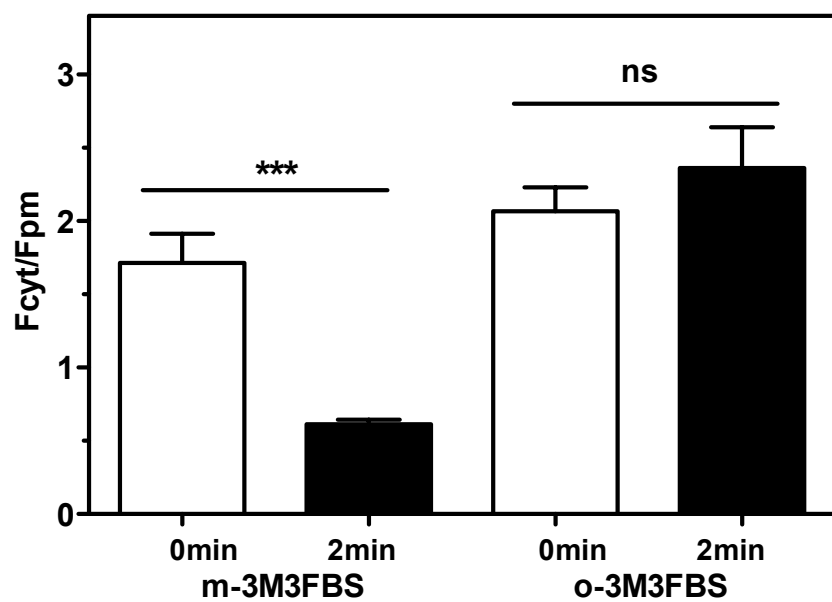
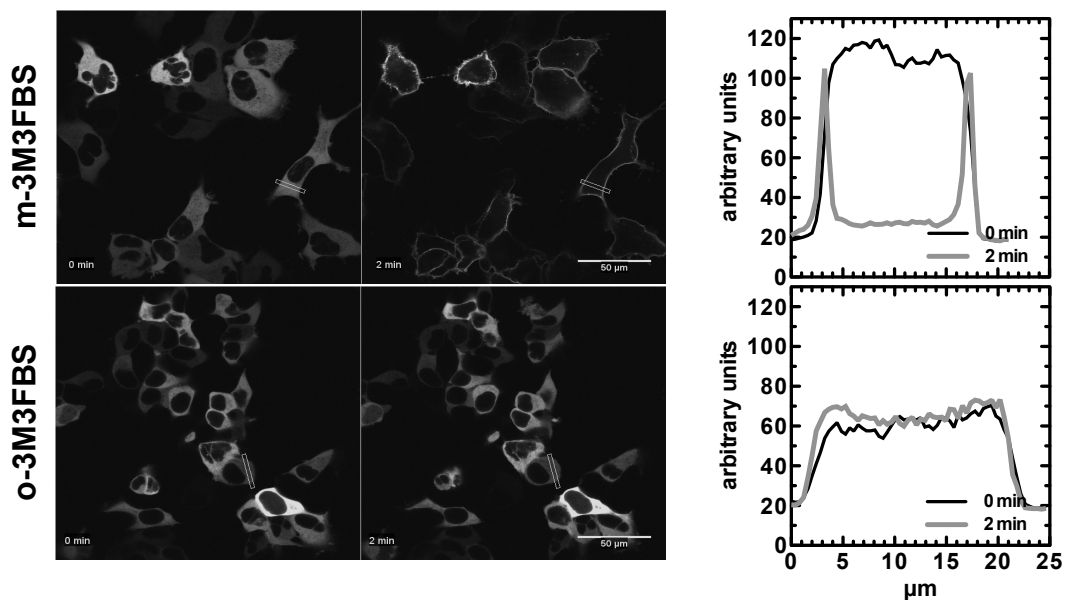


Figure S2B:

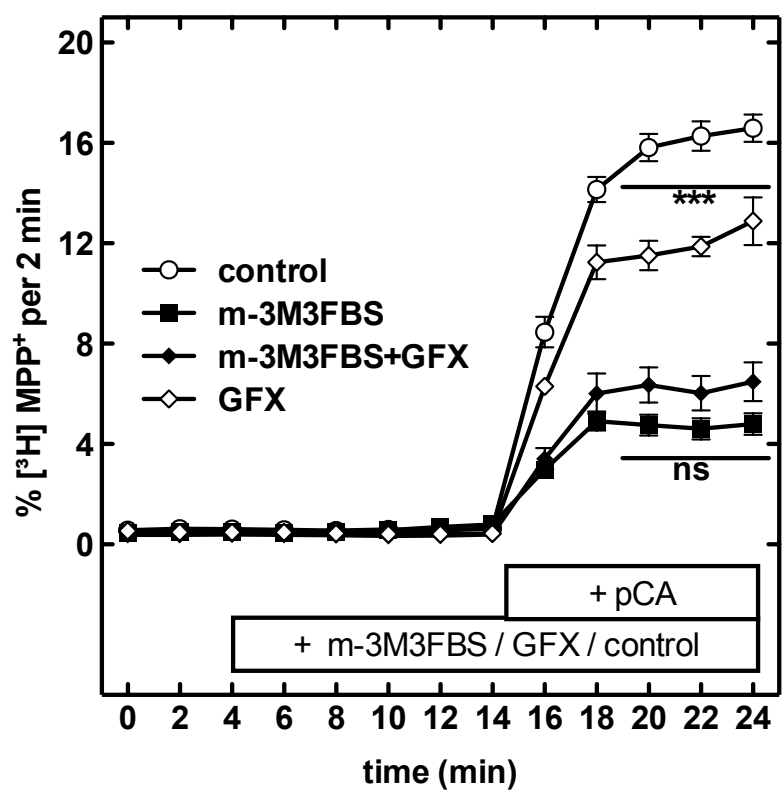


Figure S2C:

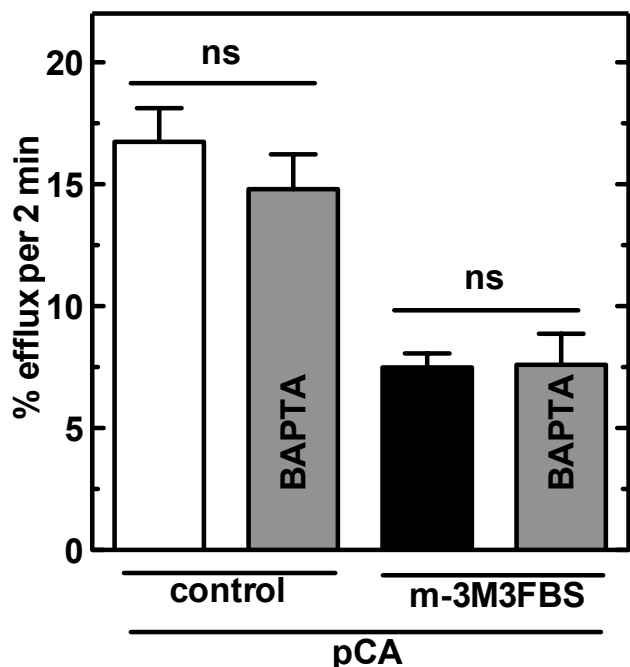


Figure S2D:

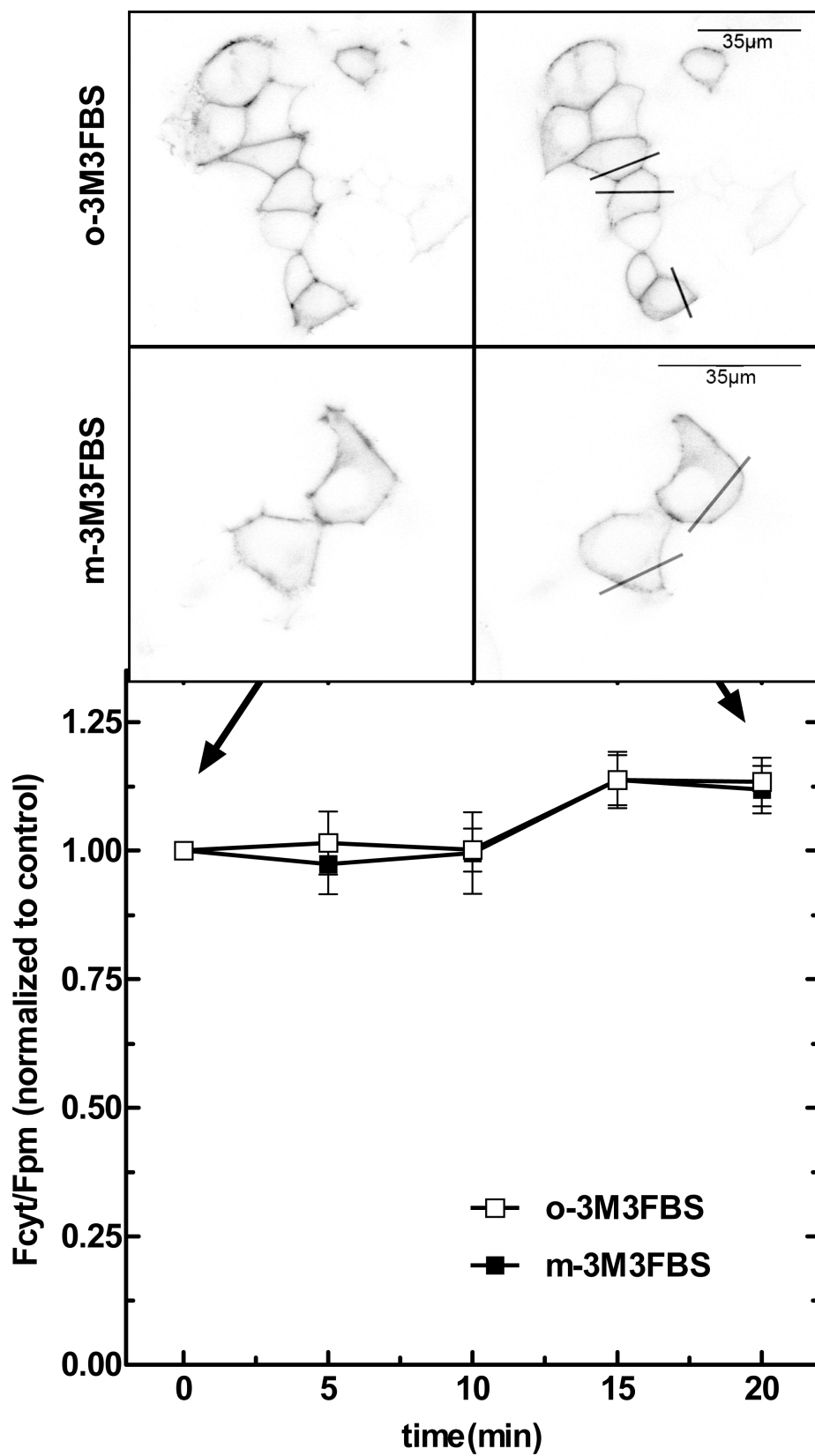


Figure S2E:

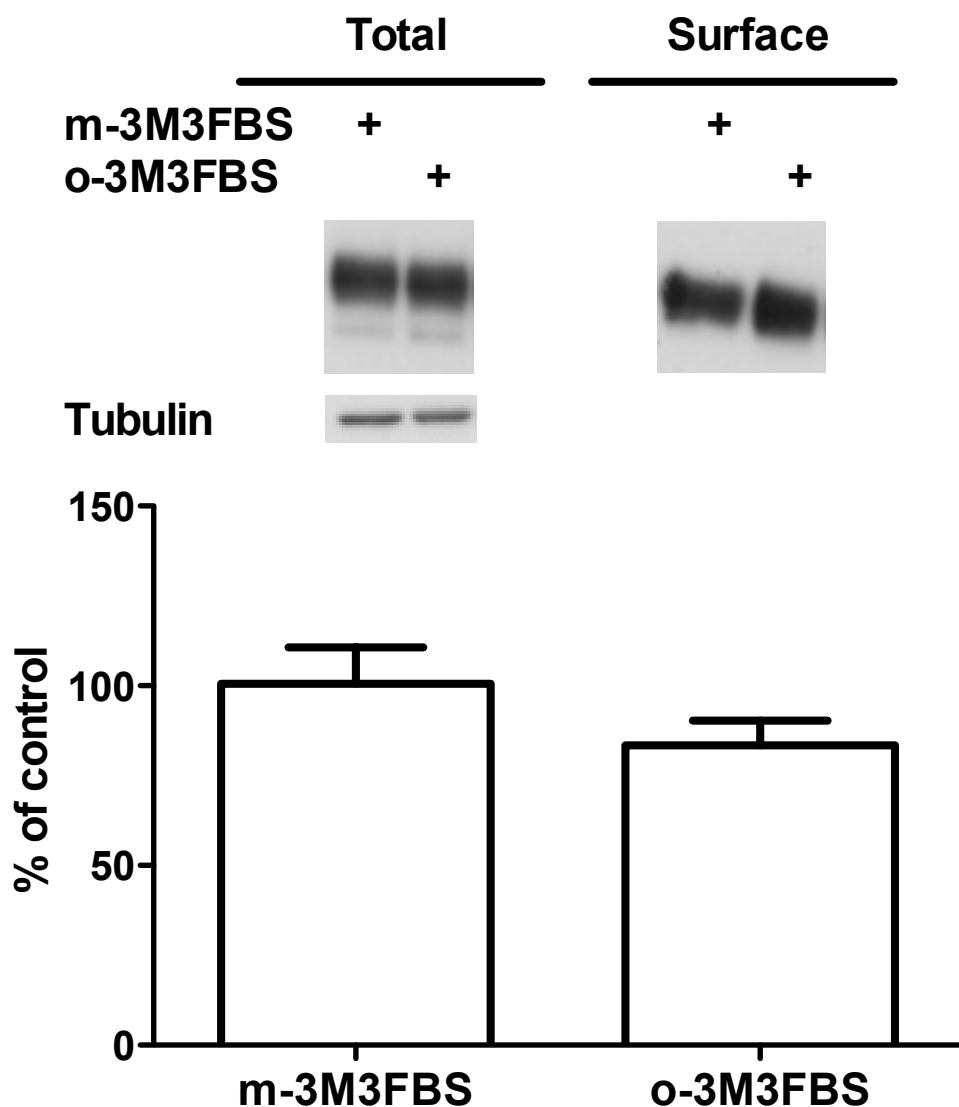


Figure S2F:

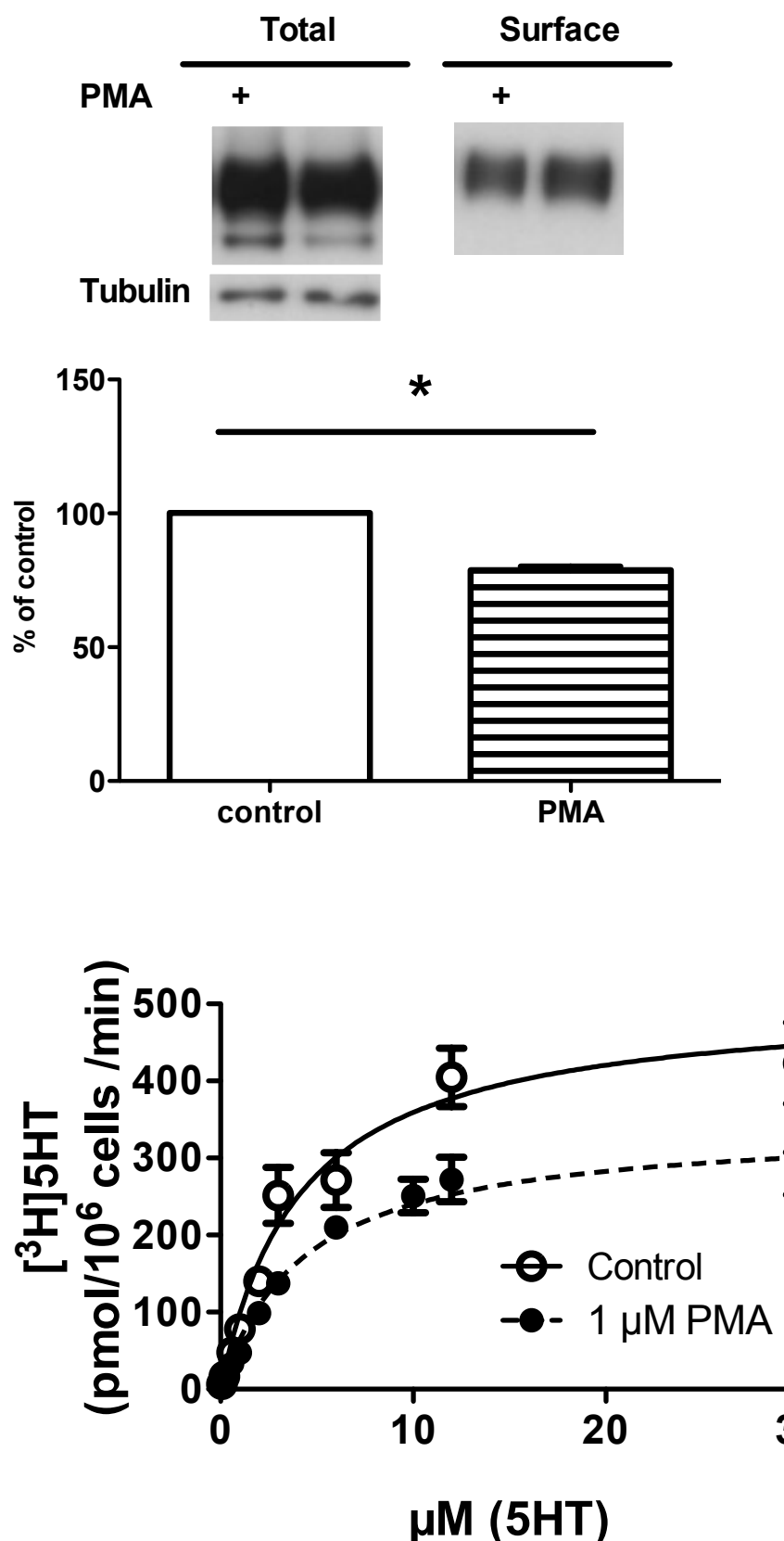


Figure S3:

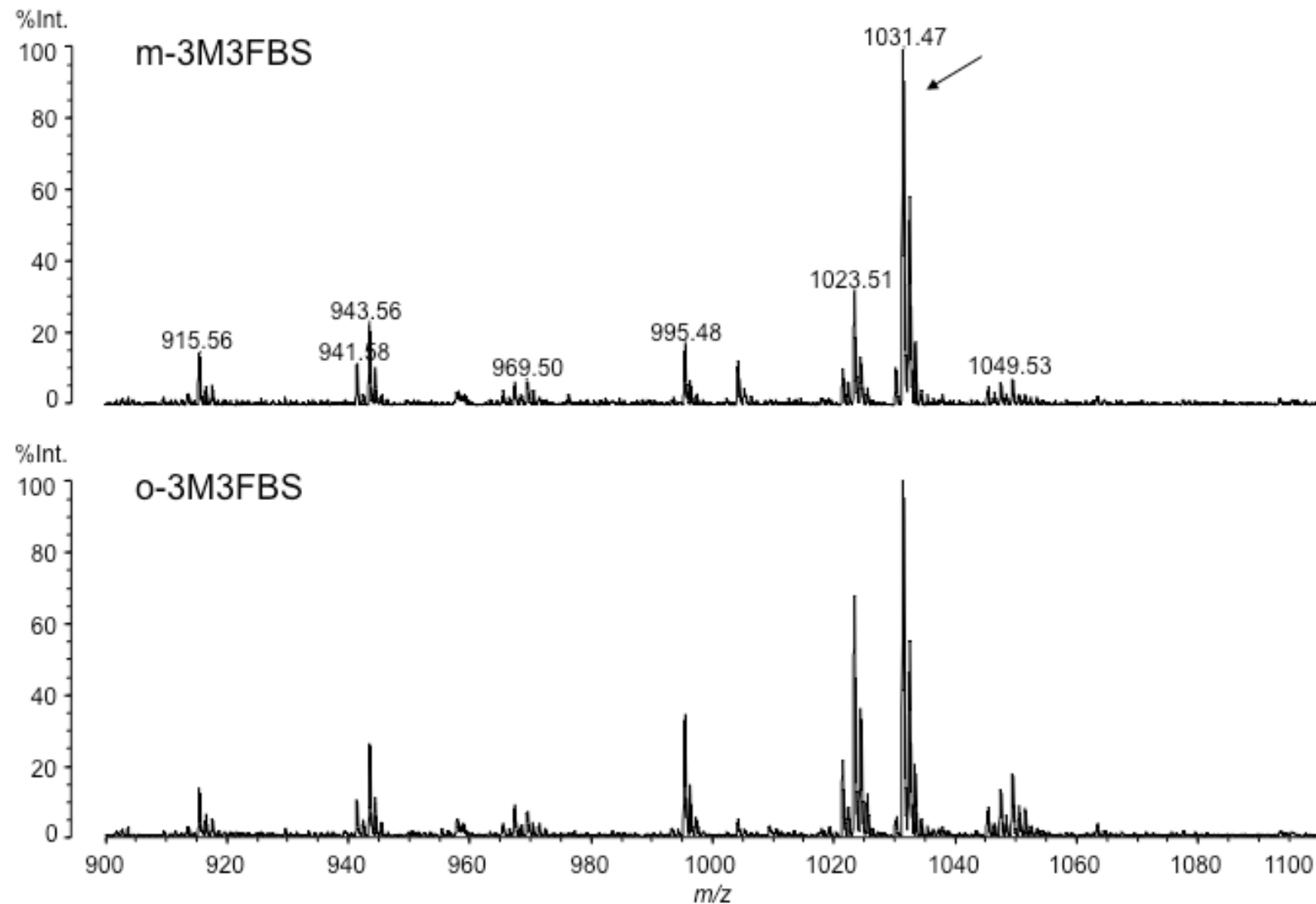


Figure S4A:

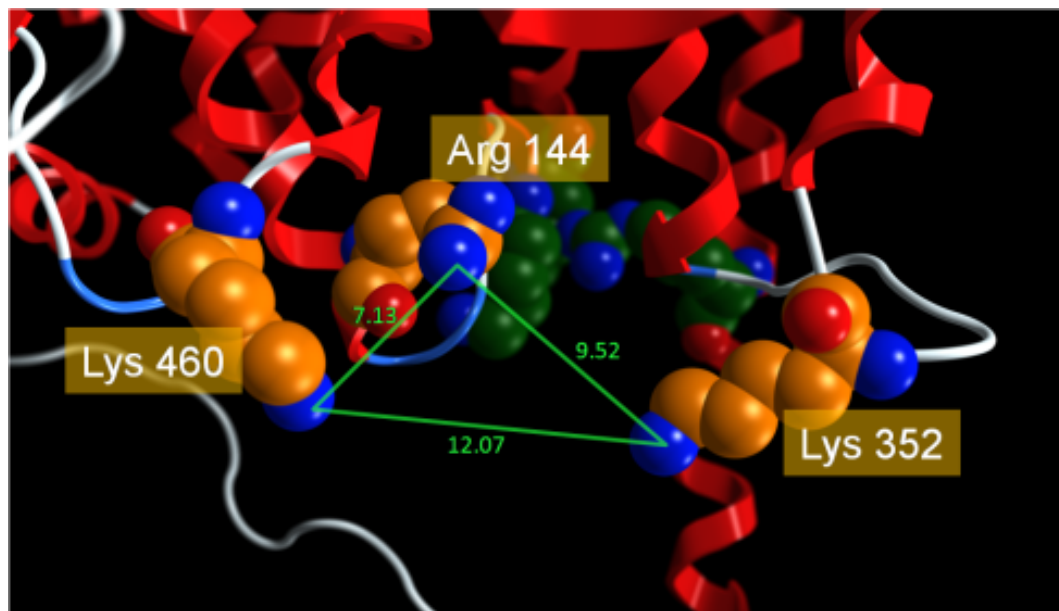
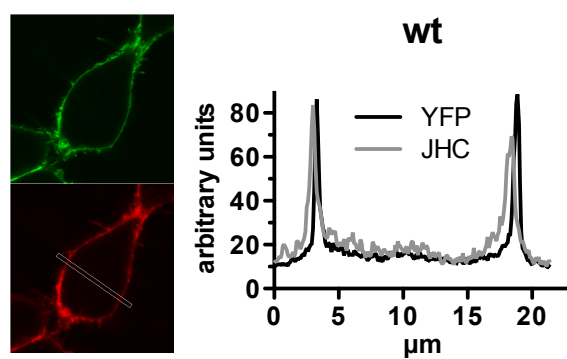
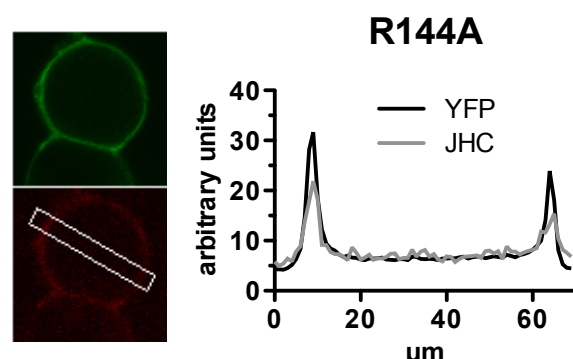


Figure S4B:

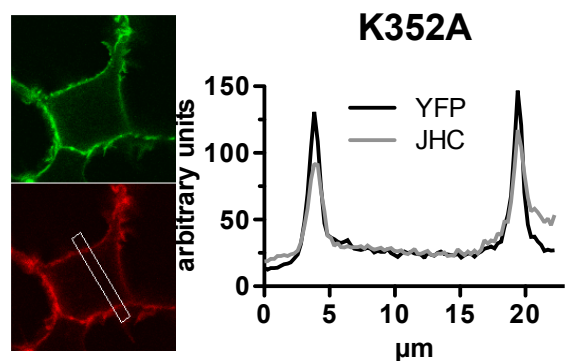
A



B



C



D

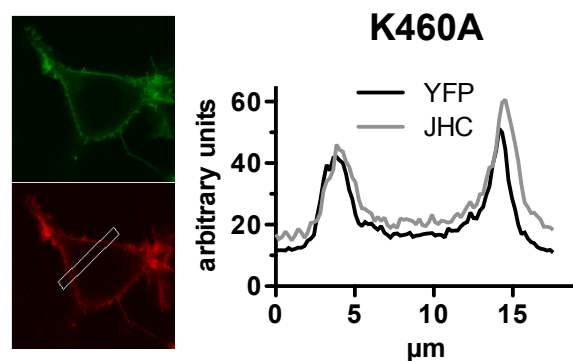
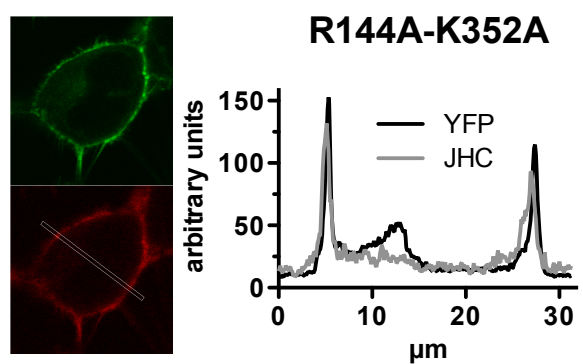
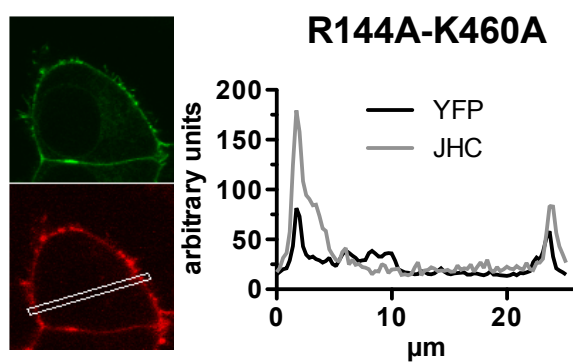


Figure S4C:

A



B



C

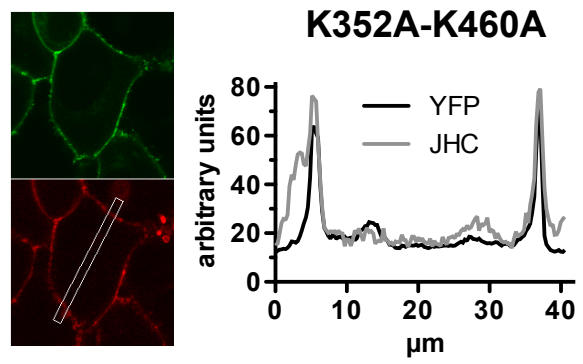


Figure S4D:

